Multi-angle aerosol optical depth retrieval method based on improved surface reflectance

Lijuan Chen[1], Ren Wang[1], Ying Fei[2], Peng Fang[2], Yong Zha[2], Haishan Chen[1*]

[1]Key Laboratory of Meteorological Disaster, Ministry of Education (KLME)/Joint International Research Laboratory of Climate and Environment Change (ILCEC)/Collaborative Innovation Center on Forecast and Evaluation of Meteorological Disasters (CIC-FEMD), Nanjing University of Information Science and Technology, Nanjing 210044, China

[2]Key Laboratory of Virtual Geographic Environment of Ministry of Education, Jiangsu Center for Collaborative Innovation in Geographical Information Resource Development and Application, College of Geographic Science, Nanjing Normal University, Nanjing 210023, China

Correspondence: Haishan Chen (haishan@nuist.edu.cn)

Abstract

Retrieval of terrestrial aerosol optical depth (AOD) has been a challenge for satellite Earth observations, mainly due to the difficulty of estimating surface reflectance caused by land-atmosphere coupling. Current satellite AOD retrieval products have low spatial resolution under complex surface processes. In this study, based on our previous studies of AOD retrieval, we further improved the estimation method of surface reflectance by establishing an error correction model, which helped us obtain more accurate AOD retrievals. We constructed a lookup table using the Second Simulation of Satellite Signal in the Solar Spectrum (6S) to achieve high-precision retrieval of AOD. The accuracy of the algorithm's retrieval was verified by AERONET (Aerosol Robotic Network) observations. The results indicated that the retrieved AOD based on the improved method of this study has advantages in terms of fewer missing AOD pixels and finer spatial resolution, compared to the MODIS AOD product and our previous estimation method. Among the nine MISR angles, the optimal correlation coefficient (R) of retrieved AOD and observed AOD can reach 0.89. Root mean square error (RMSE) and relative mean bias (RMB) can reach minimum values of 0.20 and 0.32, respectively. This study will help to further improve the accuracy of retrieving multi-angle AOD at large spatial scales and long time series.

Keywords: surface reflectance; aerosol optical depth; satellite remote sensing; MISR; MODIS

1. Introduction

Aerosols are liquid or solid particles suspended in the atmosphere, with particle diameters ranging from approximately 0.001 to 100 μm (Giles et al., 2019). Aerosols have a significant impact on the Earth's radiation budget balance, and estimating their uncertainties is challenging (Holben et al., 2001; Li et al., 2020; Berhane et al., 2021; Sun et al., 2022). As a result, the direct and indirect effects of aerosols have garnered widespread attention in the study of climate change mechanisms (Hatzianastassiou et al., 2009; Dao et al., 2014; Daniel et al., 2014; Samset et al., 2018; Li et al., 2018; Huang et al., 2021). Additionally, high concentrations of aerosols can pose a serious threat to human health (Lee et al., 2010; Dehghani et al., 2012; Mironova et al., 2015). The optical properties of aerosols include parameters such as aerosol optical depth (AOD), scattering phase function, single scattering albedo, and absorbing optical depth. Among there, AOD is an important parameter defined as the integral of aerosol extinction coefficient in the vertical direction. It describes the attenuation effect of aerosols on light and serves as an important indicator of air pollution levels. Over the past two decades, multi-channel spectrometers on geostationary and polar orbit satellites have been utilized for AOD retrieval. The AOD products obtained through satellite retrieval are widely employed in the study of atmospheric environment (Kaufman et al, 1997; Xie et al., 2019; Chen et al., 2021). Although the accuracy of AOD retrieval has continuously improved, there is still ample room for enhancing in the retrieval results over land.

Scholars have conducted studies using multi-angle sensors. Flowerdew et al. (1996) utilized Along-Track Scanning Radiometer 2 (ATSR-2) dual-angle observation data, based on the approximate condition of minimum variation of surface reflectance with wavelength, and using the assumption of independent invariance of ground features and Lambertian bodies. They simulated this by using a bidirectional reflection radiation transfer model and proposed a dual-angle algorithm (ATSR-DV) to retrieve AOD over land. Kokhanovsky et al. (2009) used the ATSR-DV algorithm to retrieve the AOD over Germany on October 13, 2005, and compared the retrieval results with MEdium-Resolution Imaging Spectrometer (MERIS) and MISR products. They indicated that the ATSR-2 algorithm is also suitable for Advanced Along-Track Scanning Radiometer (AATSR). Sundstrom et al. (2012) obtained an aerosol model of eastern China based on Aerosol Robotic Network (AERONET) observation data and used the ATSR-DV algorithm to retrieve the proportion of AOD and coarse to fine particles from AATSR data. Abdou et al. (2005) compared the MISR AOD and the Moderate-resolution Imaging Spectroradiometer (MODIS) AOD products carried by Terra using data from 62 AERONET observation sites. The results showed that over land, the MODIS AOD in the 0.470 um and 0.660 um channels was 35% and 10% higher than MISR. In coastal and desert areas, the MODIS retrieval error was relatively large, while over the ocean, in the 0.470 um and 0.660 um channels, the MISR was 0.1 and 0.05 higher than the MODIS AOD value, respectively, mainly depends on the accuracy of radiometric calibration. Martochik et al. (1997) proposed an algorithm for extracting aerosol optical parameters using MISR multi-angle observations. The results showed that in the presence of dense vegetation over land, AOD was extracted using its low reflectivity and multi-angle observations. If dense vegetation did not exist, AOD and aerosol models were determined using the reflectance function spectral contrast angle dependence relationship. As a new remote sensing tool, multi-angle remote sensing has the ability to provide aerosol characteristics such as optical depth, single scattering albedo, and phase function with sufficient precision, which is more suitable for playing its unique role in aerosol research than traditional single-angle optical remote sensing (Dubovik et al., 2019). Multi-angle remote sensing retrieval of aerosol optical properties can utilize the angle information contained in satellite signals to better separate the contributions of the surface and atmosphere, making it suitable for some bright surfaces. This provides a new approach for AOD retrieval.

Surface reflectance measures the ability of land to absorb and reflect solar radiation. On land, surface reflectance is relatively complex and is detected by satellite sensors after atmospheric scattering and absorption. Satellite observations capture a combination of there two components, making it challenging to directly separate surface reflectance from atmospheric scattering. Consequently, the simultaneous retrieval of atmospheric aerosols and surface reflectance is a primary goal in quantitative satellite remote sensing (Deuzé et al., 2001). In optical remote sensing, the blue band has shorter wavelengths and low surface reflectivity, resulting in more reflection and scattering caused by the atmosphere. Therefore, the blue band is commonly used for AOD retrieval. During the AOD retrieval process, overestimating surface reflectivity leads to underestimating AOD, while underestimating surface reflectance leads to overestimating AOD. Separating atmospherically generated reflectance from surface reflectance in apparent reflectance (reflectance at the top of the atmosphere) poses a challenge in AOD retrieval. Generally, aerosol signals are weaker compared to surface signals (Dong et al., 2023). Previous studies have shown that an intercept error of 0.01 in surface reflectance can result in a retrieval error of approximately 0.1 when using satellite remote sensing to retrieve AOD (Zhang et al., 2021). Therefore, accurate estimates of surface reflectance are crucial for reliable aerosol retrieval.

A high-precision AOD product obtained from retrieval is of great significance for monitoring changes in atmospheric pollution and providing decision-making support for pollution control. Observing the spatial distribution of AOD is crucial for daily air pollution monitoring. Additionally, aerosol particles can impact the energy balance between the land and the atmosphere by absorbing and scattering solar radiation, thereby influencing the global climate system. To enhance the accuracy and resolution of AOD retrieval, this study utilizes data from nine camera angles in the blue band of MISR L1B2T from 2016 to 2018, employing an improved retrieval algorithm. Firstly, the study analyzes the retrieval errors of MISR AOD for nine camera angles prior to the implementation of the improved retrieval approach. Secondly, an error correction model is established to rectify the estimated surface reflectance of MISR, thus improving the surface reflectance at these nine angles. The improved surface reflectance retrieval is then used to obtain highly accurate MISR AOD. Finally, the improved AOD retrieval method is validated, and its estimated results are compared with the previous retrieval.

2. MISR, MODIS, and AERONET Data

2.1 MISR data

In this study, we utilized the MISR Level 1B2 Terrain Data (MI1B2T) and extracted the radiance data using the HEGTool (HDF-EOS To GeoTIFF Conversion Tool) software. We selected the corresponding blocks, output data types, and projection based on the regional location of the 180 radiation blocks and extracted the 64th and 65th blocks covering the Yangtze River Delta region (Figure S1). Moreover, we extracted the solar zenith angle, solar azimuth angle, satellite zenith angle, and satellite azimuth angle data for 9 cameras from the angle dataset (MI1B2GEOP) and selected the corresponding blocks, output data types, and projection information. To reduce the influence of clouds, we performed cloud detection and cloud pixel removal on satellite remote sensing images with cloud pixel coverage less than 50% and used a threshold value in the blue band to remove cloud pixels. However, through repeated experiments, we found that a fixed threshold could not effectively remove the cloud pixels from the 9 angles of the MISR sensor (Figures S2 and S3). Therefore, we adopted a dynamic threshold method to remove the cloud pixels from the MISR data. Details regarding the data used in this study can be found in Table S2.

2.2 MODIS data

In this study, we utilized MODIS L1B data, including radiance data (MOD02/MYD02) and geolocation data (MOD03/MYD03). The data preprocessing, including radiometric calibration, butterfly processing, geometric correction, reprojection, and band extraction, was conducted using the MODIS Conversion Toolkit (MCTK). The MODIS BRDF/Albedo is a standard Level-3 product representing surface properties derived from MODIS instruments onboard the Terra and Aqua satellite platforms. This product has a 16-day retrieval period, and the observations from the 9th day of each 16-day cycle are weighted to generate daily data, known as the global daily surface albedo product (Hsu et al., 2004). The core dataset for MODIS BRDF product is MCD43A1.

2.3 AERONET data

This study utilized AERONET measurement stations, which employ CE-318 solar radiometers produced in France. The instrument measures direct spectral solar radiation every 3 minutes across nine channels: 340nm, 380nm, 440nm, 500nm, 670nm, 870nm, 936nm, 1020nm, and 1640nm. The measurement at the 936nm channel is used to retrieve the total atmospheric water vapor content, while the remaining channels are used to derive aerosol optical depth (AOD) with a retrieval error of approximately 0.01-0.02. Therefore, AERONET provides high-precision aerosol characteristic parameters and can be used to validate satellite-retrieved AOD (Lu et al., 2019). In this study, AOD measurements obtained from AERONET were used as ground truth to verify the accuracy of satellite remote sensing retrievals. AERONET AOD data are categorized into three quality levels: Level 1.0 (unscreened), Level 1.5 (cloud screened and quality controlled), and Level 2.0 (quality assured). The study area primarily covers the Yangtze River Delta region, where AERONET has several stations. However, continuous data were only available from the Taihu and Xuzhou-CUMT stations, while data from other stations were relatively limited in duration. Therefore, AERONET Level 1.5 AOD data with a large number of continuous and current observations were selected for validating MISR AOD retrievals.

3. Methodology

3.1 Problems in the previous surface reflectance estimation method

The accurate estimation of surface reflectance is a crucial and challenging aspect in the retrieval of AOD from satellite remote sensing data (Remer et al., 2009; Gupta et al., 2016). Previous research has identified the variation patterns of 9-angle MISR AOD (Chen et al., 2021). However, the AOD retrieved at 9 angles exhibits relatively large errors when compared to AERONET AOD (Table S3). Atmospheric correction can eliminate the effects of clouds and aerosols on data, obtaining the true surface reflectance. When using the 6S model to calculate atmospheric correction reflectance for the MISR sensor, several parameters need to be inputted, including geometric parameters, AOD, aerosol types, sensor radiance data, and sensor altitude, etc. In this study, we inputted the MISR geometric parameters and radiation data corresponding to Taihu and Xuzhou-CUMT stations, while the AOD parameter inputted was the AERONET AOD for these two stations. Through the generated linear atmospheric correction formula, we calculated the atmospheric correction reflectance for each pixel. To investigate the reasons for the higher AOD values retrieved from the 9 MISR angles, this study compared the MISR atmospheric correction reflectance and MISR surface reflectance at the pixel location (Figure 1) (MISR surface reflectance calculation method referenced Chen et al. (2021)). It was observed that the MISR surface reflectance was relatively lower compared to the MISR atmospheric correction reflectance. As a result, the retrieved MISR AOD values were higher compared to AERONET AOD. Therefore, it is necessary to establish a correction model to adjust the MISR surface reflectance and improve the retrieval accuracy of MISR AOD.

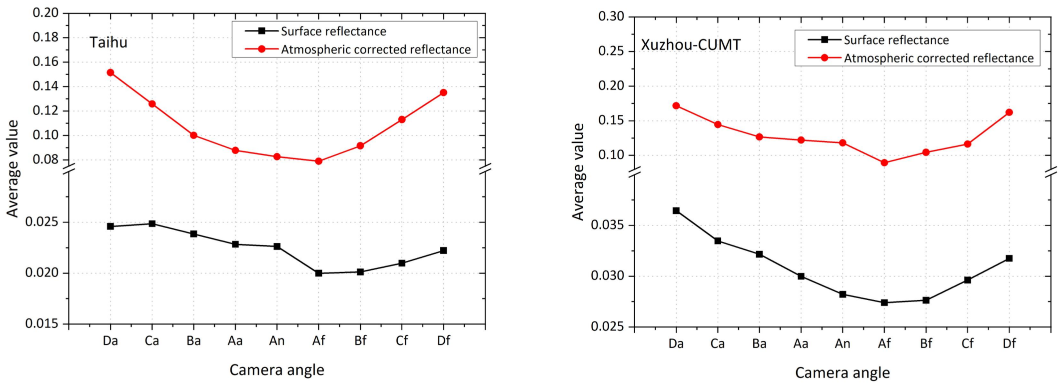

Figure 1. Comparison of MISR surface reflectance with atmospheric corrected reflectance in the blue band (At the pixel locations of Taihu and Xuzhou-CUMT sites).

3.2 Improved surface reflectance estimation method

To develop a correction model that improves the surface reflectance, the design scheme of this study is shown below:

(1) Calculation of MODIS atmospheric corrected reflectance

The atmospheric correction of MODIS L1B was carried out using the 6S model to obtain MODIS atmospheric corrected reflectance. When using the 6S model to calculate the atmospheric correction reflectance of the MODIS sensor, several parameters need to be provided, including geometric parameters, AOD, atmospheric models, aerosol types, sensor radiance data, sensor altitude, and spectral parameters. In this study, we used the MODIS geometric parameters and radiance data corresponding to the Taihu and Xuzhou-CUMT sites. The AOD parameter was obtained from the AERONET AOD data measured at these two sites. The atmospheric models chosen were mid-latitude winter and mid-latitude summer to account for seasonal variations in atmospheric transmission. The aerosol type selected was continental aerosol since it is typically found in the Yangtze River Delta region. The sensor altitude was set to the height of satellite observations. The spectral parameters were defined based on the wavelength bands of the MODIS sensor. By providing these parameters, we can utilize the 6S model to calculate the atmospheric correction reflectance of the MODIS sensor.

(2) Calculation of surface bidirectional reflectance

We utilized the MODIS BRDF/Albedo product MCD43A1 data and employed the Ross-Li model to simulate surface bidirectional reflectance under MODIS and MISR observation geometries. The linear kernel-driven BRDF model comprises three essential parameters: the nadir-view reflectance, and the weighting coefficients for the two kernel functions. The model can be computed using formulas 1-9.

$$BRDF(\theta_s,\theta_v,\phi) = f_{iso}(\Lambda) + f_{vol}(\Lambda)K_{vol}(\theta_s,\theta_v,\phi) + f_{geo}(\Lambda)K_{geo}(\theta_s,\theta_v,\phi) \quad (1)$$

$$K_{vol}(\theta_s,\theta_v,\phi) = \frac{(\pi/2-\xi)\cos\xi + \sin\xi}{\cos\theta_s + \cos\theta_v} - \frac{\pi}{4} \quad (2)$$

$$K_{geo}(\theta_s,\theta_v,\phi) = O(\theta_s,\theta_v,\phi) - \sec\theta'_s - \sec\theta'_v + \frac{1}{2}(1+\cos\xi')\sec\theta'_s\sec\theta'_v \quad (3)$$

$$O(\theta_s,\theta_v,\phi) = \frac{1}{\pi}(t - \sin t\cos t)(\sec\theta'_s + \sec\theta'_v) \quad (4)$$

$$\cos t = \frac{h}{b}\frac{\sqrt{D^2 + (\tan\theta'_s\tan\theta'_v\sin\phi)^2}}{\sec\theta'_s + \sec\theta'_v} \quad (5)$$

$$D = \sqrt{\tan^2\theta'_s + \tan^2\theta'_v - 2\tan\theta'_s\tan\theta'_v\cos\phi} \quad (6)$$

$$\cos\xi' = \cos\theta'_s\cos\theta'_v + \sin\theta'_s\sin\theta'_v\cos\phi \quad (7)$$

$$\theta'_s = \tan^{-1}(\frac{b}{r}\tan\theta_s) \quad (8)$$

$$\theta'_v = \tan^{-1}(\frac{b}{r}\tan\theta_v) \quad (9)$$

In the aforementioned equation, $BRDF(\theta_s,\theta_v,\phi)$ represents the bidirectional reflectance of the surface, while θ_s, θ_v, and ϕ denote the solar zenith angle, view zenith angle, and relative azimuth angle, respectively. Λ stands for the bandwidth, while $K_{vol}(\theta_s,\theta_v,\phi)$ and $K_{geo}(\theta_s,\theta_v,\phi)$ represent the volumetric scattering kernel and geometric optical scattering kernel, respectively. These terms are all functions of the incident and viewing angles. f_{iso}, f_{vol}, and f_{geo} correspond to the weights assigned to isotropic scattering, volumetric scattering, and geometric optical scattering in the reflectance, which serve as coefficients for their respective kernel functions. ξ represents the scattering angle, while b, h, and r represent the vertical radius, horizontal radius, and height of the sphere's center, respectively. Based on empirical values, these three parameters can be considered as fixed values. Within the production process of MODIS BRDF model parameter products, the following relationships exist among these parameters: h/b=2 and b/r=1 (Schaaf et al., 1999). By utilizing extrapolation with kernel functions, the surface's bidirectional reflectance can be computed under arbitrary solar incident and satellite viewing directions using the aforementioned equation.

(3) Improved calculation of surface reflectance by MISR

The new estimated MISR surface reflectance based on the MODIS atmospheric correction was calculated by bringing the MODIS atmospheric correction reflectance into Eq. 10 and Eq. 11. The MISR surface reflectance was combined with the newly estimated MISR surface reflectance, and a regression was fitted (with 60% of the overall sample data randomly selected) to create a surface reflectance error correction model, as shown in the following formula:

$$\rho(\theta_s,\theta_v,\phi)_{MISR\_a} = \rho(\theta_s,\theta_v,\phi)_{MODIS\_at} \times \frac{BRDF(\theta_s,\theta_v,\phi)_{MISR}}{BRDF(\theta_s,\theta_v,\phi)_{MODIS}} \quad (10)$$

In Eq. 10, $BRDF(\theta_s,\theta_v,\phi)_{MISR}$, $BRDF(\theta_s,\theta_v,\phi)_{MODIS}$ are BRDFs obtained at MISR and MODIS angles, respectively. θ_s is the solar zenith angle, θ_v is the satellite zenith angle, and ϕ is the relative azimuth angle. $\rho(\theta_s,\theta_v,\phi)_{MISR\_a}$ is the surface reflectance of MODIS at the geometric observation angle of MISR, and $\rho(\theta_s,\theta_v,\phi)_{MODIS\_at}$ is the MODIS atmospheric corrected reflectance.

This study selected spectral data containing 28 typical features of different types of vegetation, soil and water bodies from five standard spectral libraries that come with the ENVI software. The surface reflectance of different features in the blue bands of MODIS and MISR was calculated using formulas (Chen et al., 2021).

$$\rho(\theta_s,\theta_v,\phi)_{MISR} = \rho(\theta_s,\theta_v,\phi)_{MISR\_a} \times 0.9834 - 0.0081 \quad (11)$$

The New MODIS surface reflectance ($\rho(\theta_s,\theta_v,\phi)_{MISR\_a}$) at the MISR angle obtained from Eq. 11 is converted to the MISR surface reflectance by Eq. 11.

The MISR surface reflectance estimated by Eq. 11 is transformed using an error correction model to obtain the final improved MISR surface reflectance. The improved MISR surface reflectance will be used in the retrieval of the AOD. The MISR correction model was developed by fitting a linear regression of the previously estimated MISR surface reflectance based on the MODIS V5.2 algorithm to the MISR surface reflectance estimated based on the MODIS atmospheric correction (60% of the data were randomly selected) as shown in Eq.12. The previously estimated 9-angle MISR surface reflectance was error-corrected by Eq. 12 to obtain the improved surface reflectance for the 9 angles of the MISR sensor, which was ultimately used to perform the MISR AOD retrieval for the 9 angles.

$$\rho(\theta_s,\theta_v,\phi)_{MISR-b}{}^{*} = \rho(\theta_s,\theta_v,\phi)_{MISR} \times 0.9209 + 0.0409 \quad (12)$$

Where $\rho_{MISR-b}{}^{*}$ is the improved MISR surface reflectance in Eq. 12.

3.3 Flow of improved multi-angle AOD retrieval

The flow of the improved surface reflectance algorithm for this study is shown in Figure 2. The MODISL1B data were first atmospherically corrected using 6S. Then, the MISR surface reflectance estimated from previous study was combined with the new MISR surface reflectance estimated from Eq. 11 to build a MISR error correction model for obtaining the improved MISR surface reflectance (Chen et al., 2021). The study retrieved the MISR AOD for nine camera angles using improved MISR surface reflectance. We validated the improved MISR AOD with AERONET AOD. We compared the improved AOD with the previously retrieved AOD and analyzed the accuracy and spatial distribution trends of the improved AOD. The AOD retrieval method used in this study is based on chen et al. (2021). In our study, we used continental aerosols for AOD retrieval and atmospheric correction using the 6S model. The selection of an appropriate aerosol type is crucial for obtaining accurate aerosol optical depth. Previous studies have shown that continental aerosols can be used to estimate aerosol optical depth in the Yangtze River Delta region (He et al., 2015). We employed the same aerosol type for AOD retrieval and atmospheric correction and utilized the 6S model for atmospheric correction. Thus, this study did not consider the potential error propagation caused by aerosol type and atmospheric correction.

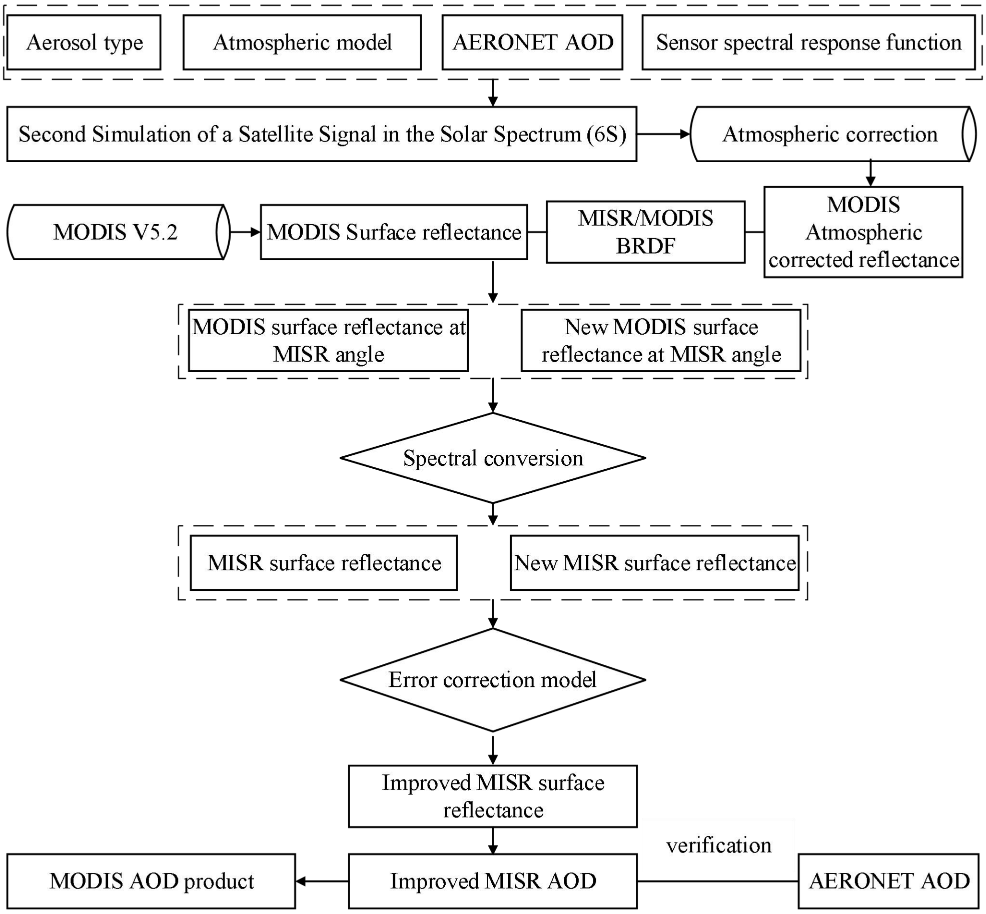

Figure 2. Flow chart of the improved MISR surface reflectance algorithm

4. Results and discussion

4.1 Improved MISR surface reflectance variation characteristics

The estimated MISR surface reflectance, the MISR atmospherically corrected reflectance, and the improved MISR surface reflectance are presented in Figure 3. These values represent the average of all sample data collected at the corresponding locations at the two sites, Taihu and Xuzhou-CUMT, during the valid dates of 2016-2018. It is worth noting that at both the Taihu and Xuzhou-CUMT sites, the nine-camera-angle MISR-improved surface reflectance values are generally higher than the MISR surface reflectance and lower than the MISR atmospherically corrected reflectance. The nine-camera-angle MISR surface reflectance values ranged from 0.02 to

0.04. On average, the improved surface reflectance values higher than the previously estimated MISR surface reflectance.

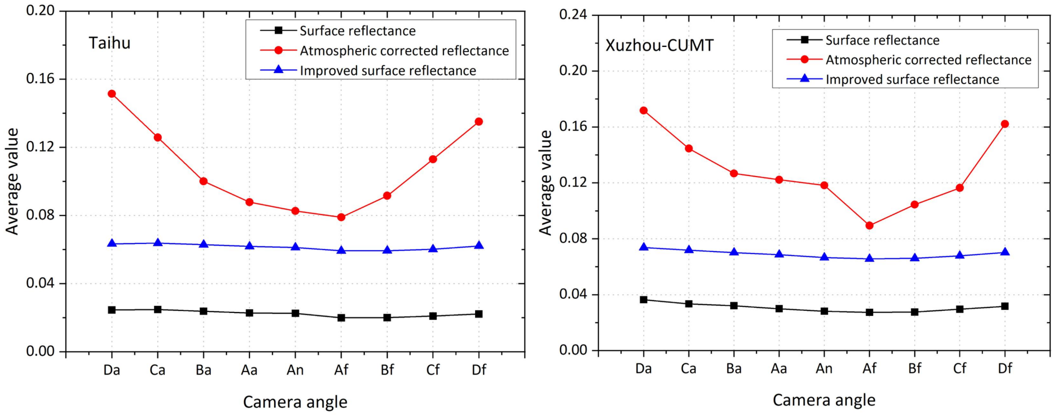

Figure 3. The comparison of MISR surface reflectance, atmospheric corrected reflectance and improved surface reflectance in the blue band (This is the multi-year average of the sample data for the two sites in Taihu and Xuzhou-CUMT).

To clarify the trend of the improved surface reflectance, the study conducted a time-series analysis of the MISR surface reflectance and the improved surface reflectance (Figure 4). It is evident from the analysis that the improved MISR surface reflectances are consistently higher than the previously estimated MISR surface reflectances. The MISR surface reflectance values generally range from 0-0.05, while the improved surface reflectance values range approximately from 0.05-0.1. Overall, there has been an increase in the improved surface reflectance values.

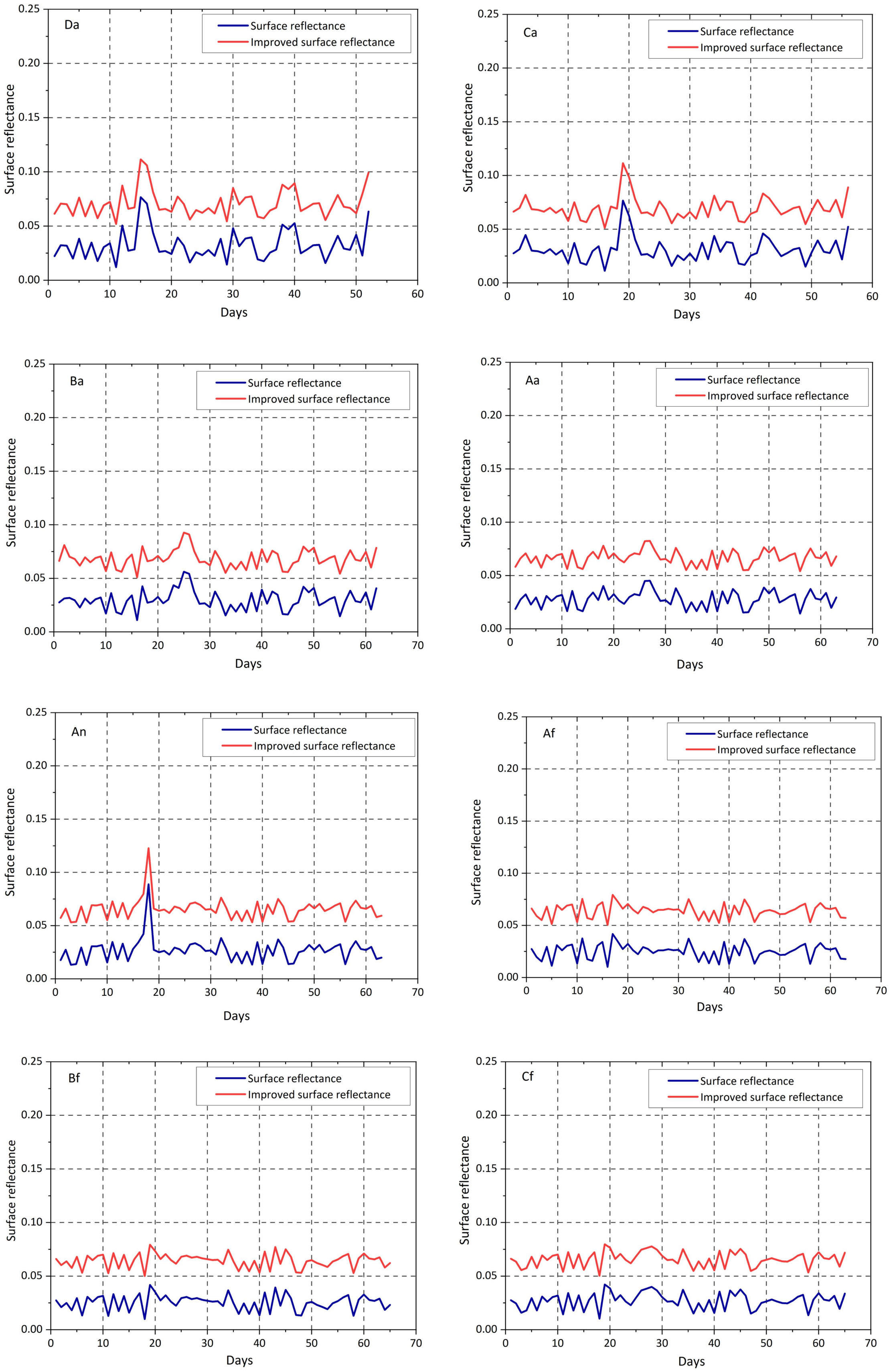
Da
Ca
Ba
Aa
An
Af
Bf
Cf
Surface reflectance
Improved surface reflectance
Days
0.00
0.05
0.10
0.15
0.20
0.25
0
10
20
30
40
50
60
70

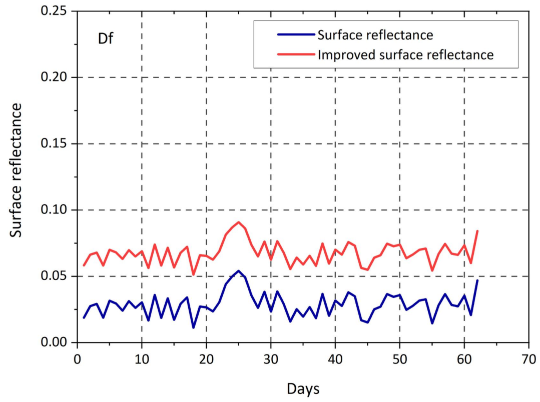

Figure 4. Surface reflectance time series of MISR sensors in the blue band at 9 observation angles. (The order of time from front to back for 9 angles is shown in Table S2)

4.2 Results of the Improved MISR AOD retrieval

MISR AOD values for 2016-2018 were obtained using an improved surface reflectance retrieval. The study presents the retrieval results from nine camera observation angles of the MISR sensor on 12 June 2018 (Figure 5). From the spatial distribution of AOD, it is evident that the retrieval results in the study area do not exceed a value of 1. The overall spatial distribution trend is generally consistent with the results before the improvement (Chen et al., 2021), but there are differences in the magnitude of the values. Values in the north-eastern and southern regions range from 0.5 to 1, indicating poor air quality to some extent in these areas. The AOD values retrieved from the five camera observation angles, Ba, Aa, An, Af, and Bf, fall within the approximate range of 0.25-0.5. In the central region, the AOD values from the four camera observation angles, Da, Ca, Cf, and Df, are mostly in the range of 0-0.25. The values suggest that the air quality in the central region is generally good, with some areas experiencing light air pollution. The higher AOD in the southern part of Shandong Province and the northern part of Jiangsu Province may be attributed to increased local aerosol emissions resulting from human activities.

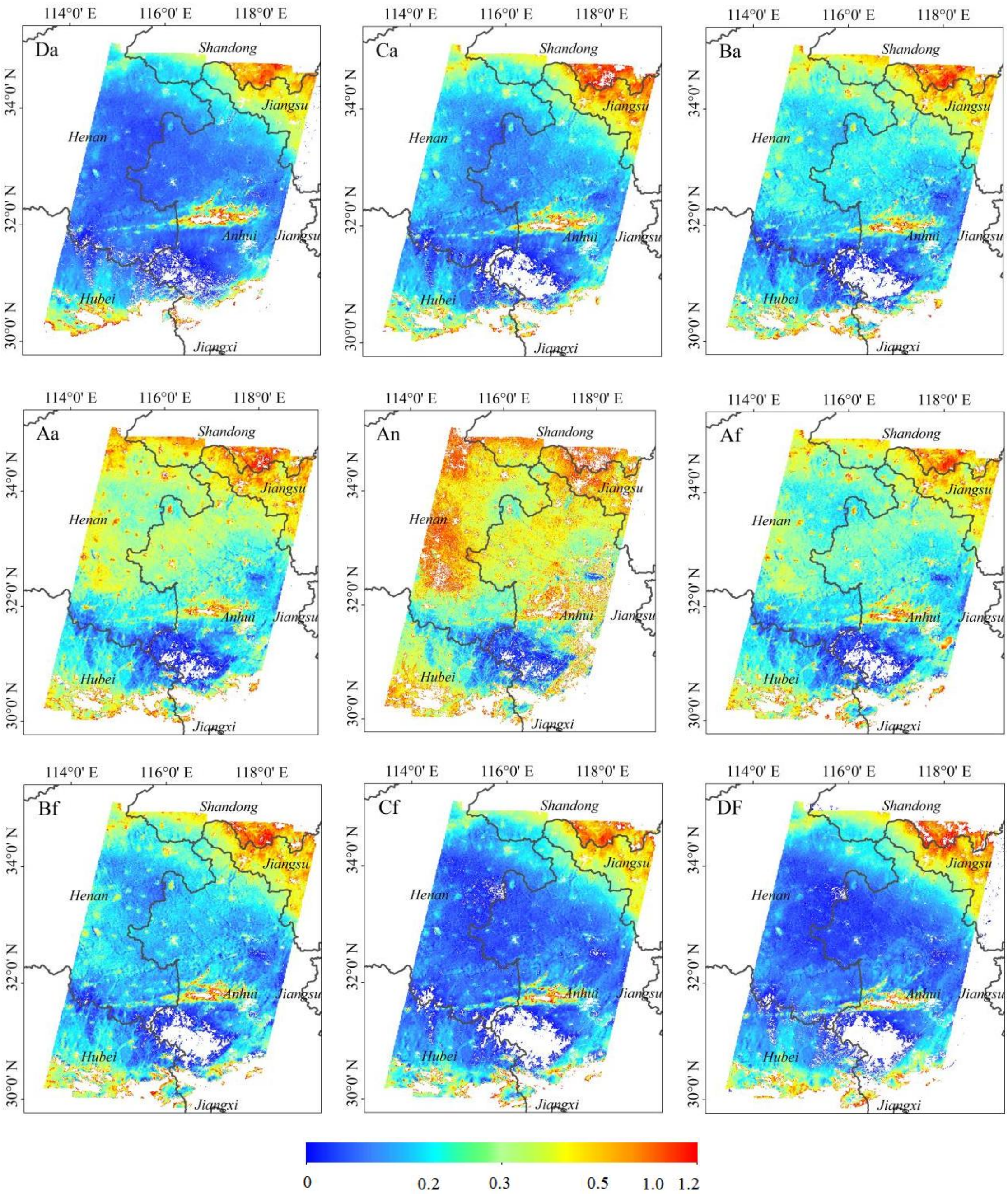

Figure 5. Plot of AOD 550nm retrieval results for the improved MISR 9 camera angles on 12 June 2018.

The study validates our improved MISR AOD spatial distribution results by comparing them with MODIS AOD products on the same date (Figure 6). The MODIS AOD products have a resolution of 3km. It can be observed that the trend of the spatial distribution of MODIS AOD products is consistent with the improved MISR AOD. However, the MODIS AOD product has more missing data, which can be avoided by using AOD obtained from the retrieval of the improved algorithm. Additionally, the AOD retrieval through the improved algorithm has a higher resolution when compared to the image quality of the MISR AOD product.

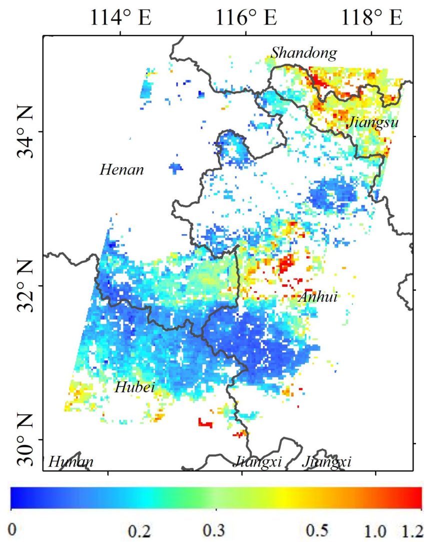

Figure 6. MODIS AOD 550nm product spatial distribution on June 12, 2018

4.3 Verification of the improved MISR AOD

There are many AERONET sites in the Yangtze River Delta region, but currently, only the Taihu and Xuzhou-CUMT sites continue to provide data, and other sites have a limited time frame for obtaining data. Therefore, the Taihu and Xuzhou-CUMT sites, which have more data, were selected for verification. To verify the retrieved MISR AOD, we selected effective AOD records in the 550nm band within a 30-minute interval between the AERONET ground observation site and the Terra satellite. The 9 camera views of MISR require approximately 7 minutes to observe the same geographical location, with relatively short intervals. Therefore, we used the calculated AERONET AOD average as the approximate truth value and compare it with the retrieved MISR AOD to verify and reduce errors caused by time difference. In terms of space, we selected pixels observed by the MISR sensors from 9 angles and compared them with the nearest data observed by AERONET, which can reduce errors caused by spatial differences. As the solar photometer does not have a 550nm wavelength that corresponds to the retrieval results, the AOD at 550nm was calculated by applying Angstrom (Eq. 13).

$$\tau(\lambda) = \beta\lambda^{-\alpha} \quad (13)$$

In the formula, $\tau(\lambda)$ is the AOD at wavelength λ, β is the concentration of the entire atmospheric aerosol, and α is the wavelength index of Angstrom.

In this study, four parameters will be used to assess the accuracy of the remotely sensed AOD dataset, namely the correlation coefficient (R), the root mean square error (RMSE), p-value and the relative mean bias (RMB). The specific calculation principles for the three parameters R, RMSE and RMB are shown in Eq. 14-16. The validation results of this study's improved AOD dataset from 2016-2018 at Taihu and Xuzhou-CUMT sites are shown in Figure 7 and Figure 8.

In general, the scatter plot is distributed above and below the 1:1 line. R is a parameter used to characterize the correlation between the remote sensing retrieval results and the ground-based retrieval results. At the Taihu site, R reach up to 0.89, and at the Xuzhou-CUMT site, R reach up to 0.85. The RMSE is a parameter used to characterize the absolute error of the remote sensing retrieval results, with a minimum root mean square error of 0.21 at the Taihu site and 0.20 at the Xuzhou-CUMT site. RMB is the parameter used to characterize the relative error of the remote sensing retrieval results, with a minimum RMB of 0.52 at the Taihu site and 0.32 at the Xuzhou-CUMT site. In summary, by comparing the results with the validation of the AOD scatter plot before the improvement, the accuracy of the nine camera observation angles at both sites has improved after the improvement (Table 1). In Table 1, R represents the correlation between the old AOD retrieval results and AERONET AOD. RMB represents the relative deviation between the old algorithm-retrieved AOD and AERONET AOD. Improved R represents the correlation between the improved AOD retrieval results and AERONET AOD. Improved RMB represents the relative deviation between the AOD retrieved using the improved algorithm and AERONET AOD.

$$R = \frac{\sum_{i=1}^{N}(A_i - \overline{A})(A_i^{'} - \overline{A^{'}})}{\sqrt{\sum_{i=1}^{N}(A_i - \overline{A})^2 \sum_{i=1}^{N}(A_i^{'} - \overline{A^{'}})^2}} \quad (14)$$

$$RMSE = \sqrt{\sum_{i=1}^{N}(A_i - A_i^{'})^2 / N} \quad (15)$$

$$RMB = \sum_{i=1}^{N}(A_i - A_i^{'}) / N \quad (16)$$

where A_i is the retrieve MISR AOD, $A_i^{'}$ is the corresponding AERONET AOD, $\overline{A}$ and $\overline{A^{'}}$ are the mean values of the retrieve MISR AOD and AERONET AOD, respectively. N is the number of valid matching results for AERONET AOD and MISR AOD.

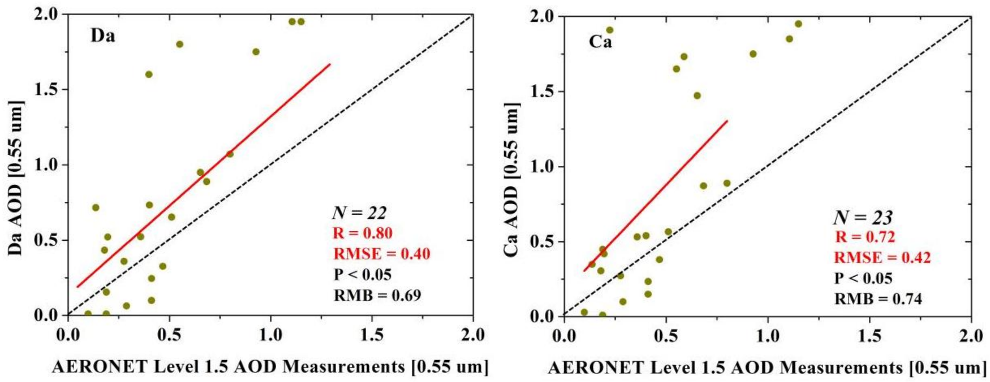

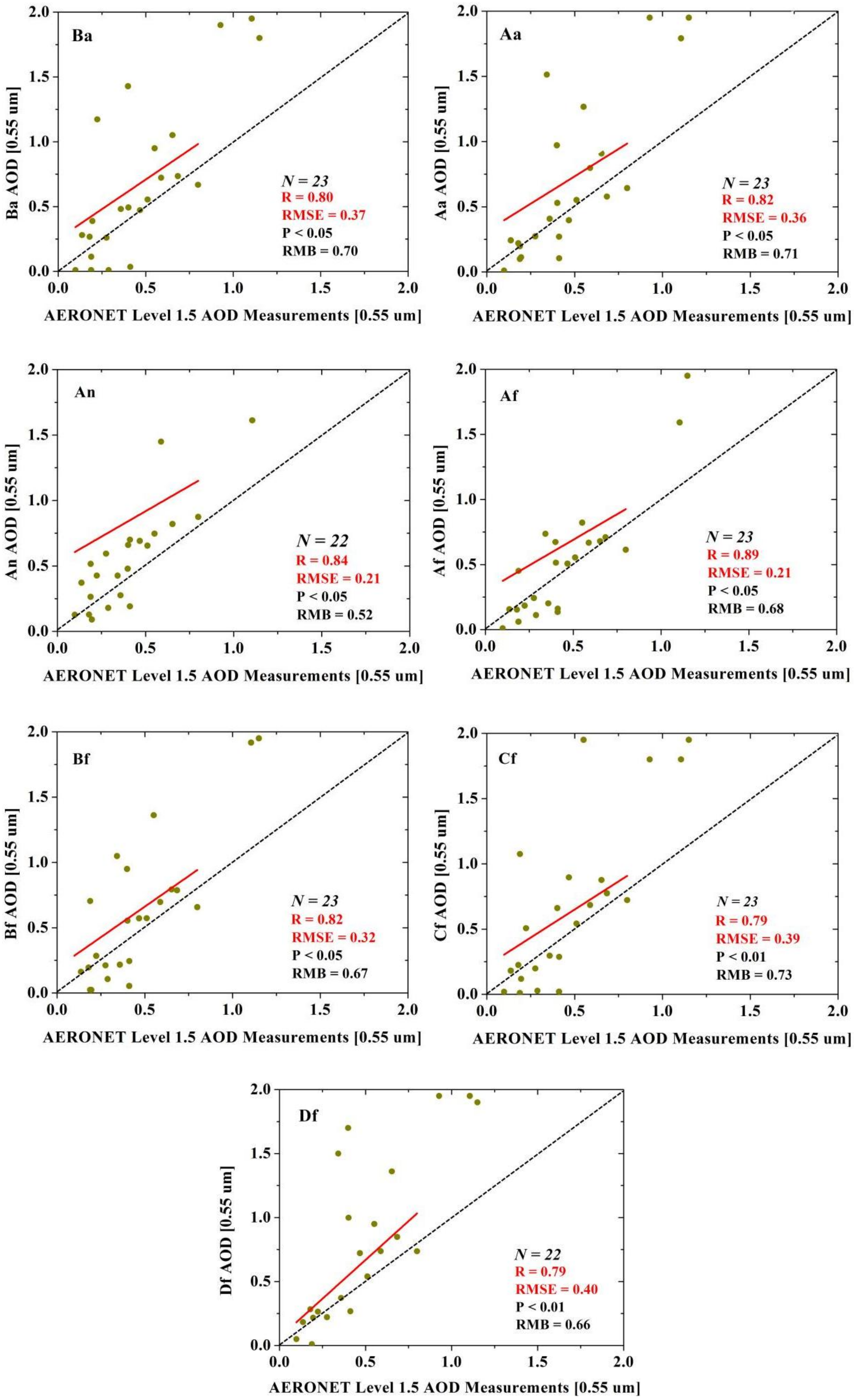

Figure 7. Comparison between improved MISR AOD and AERONET AOD at Taihu site (N is the number of verification points, red line represents a linear fitting line).

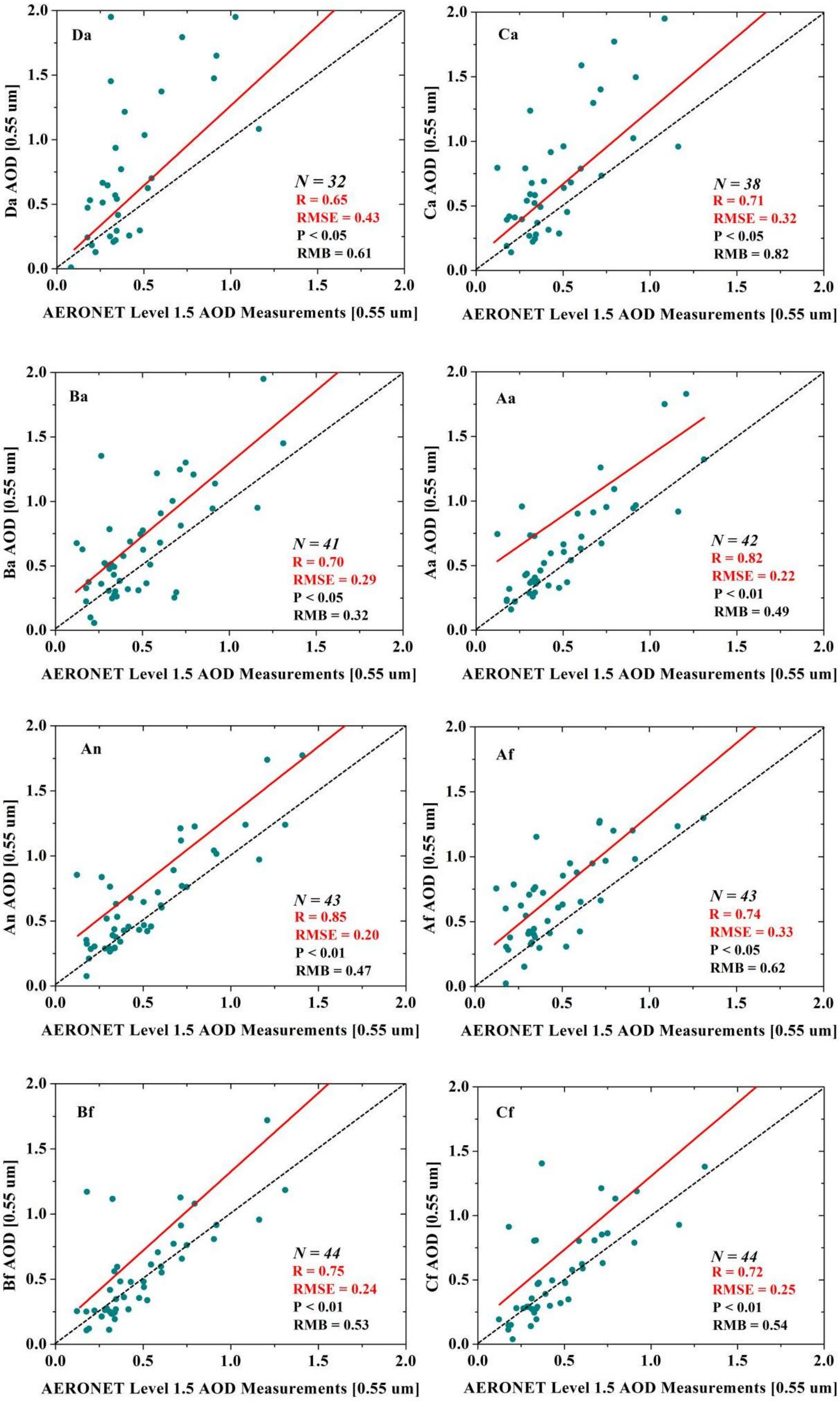

Da
N = 32
R = 0.65
RMSE = 0.43
P < 0.05
RMB = 0.61
Da AOD [0.55 um]
AERONET Level 1.5 AOD Measurements [0.55 um]
Ca
N = 38
R = 0.71
RMSE = 0.32
P < 0.05
RMB = 0.82
Ca AOD [0.55 um]
AERONET Level 1.5 AOD Measurements [0.55 um]
Ba
N = 41
R = 0.70
RMSE = 0.29
P < 0.05
RMB = 0.32
Ba AOD [0.55 um]
AERONET Level 1.5 AOD Measurements [0.55 um]
Aa
N = 42
R = 0.82
RMSE = 0.22
P < 0.01
RMB = 0.49
Aa AOD [0.55 um]
AERONET Level 1.5 AOD Measurements [0.55 um]
An
N = 43
R = 0.85
RMSE = 0.20
P < 0.01
RMB = 0.47
An AOD [0.55 um]
AERONET Level 1.5 AOD Measurements [0.55 um]
Af
N = 43
R = 0.74
RMSE = 0.33
P < 0.05
RMB = 0.62
Af AOD [0.55 um]
AERONET Level 1.5 AOD Measurements [0.55 um]
Bf
N = 44
R = 0.75
RMSE = 0.24
P < 0.01
RMB = 0.53
Bf AOD [0.55 um]
AERONET Level 1.5 AOD Measurements [0.55 um]
Cf
N = 44
R = 0.72
RMSE = 0.25
P < 0.01
RMB = 0.54
Cf AOD [0.55 um]
AERONET Level 1.5 AOD Measurements [0.55 um]

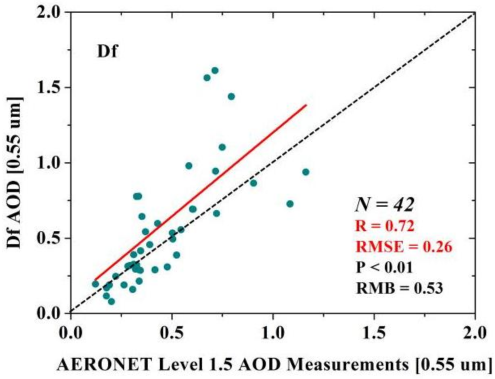

Figure 8. Comparison between improved MISR AOD and AERONET AOD at Xuzhou-CUMT site (N is the number of verification points, red line represents a linear fitting line).

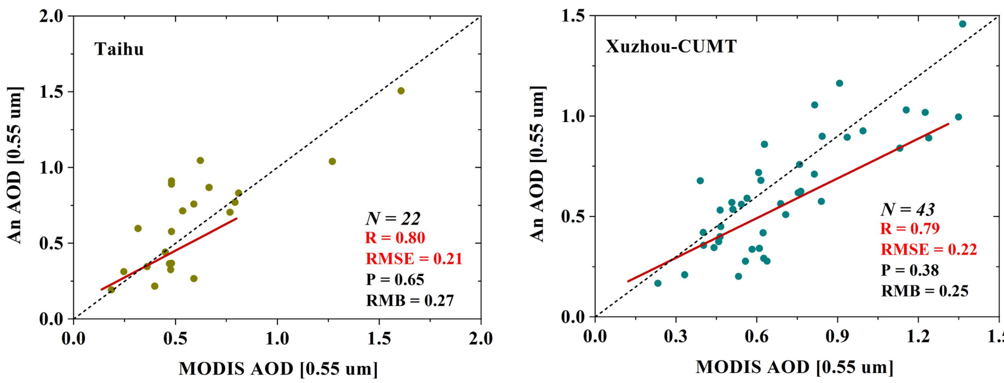

Figure 9. Comparison of validation of retrieved AOD with MODIS AOD product

Table 1. Precision comparison of MISR AOD and AERONET AOD before and after improvement

Site	Angle	R	RMB	Improved R	Improved RMB
Taihu	Da	0.77	1.08	0.80	0.69
	Ca	0.70	1.00	0.72	0.74
	Ba	0.77	0.61	0.80	0.70
	Aa	0.81	0.68	0.82	0.71
	An	0.45	1.22	0.84	0.52
	Af	0.72	0.87	0.89	0.68
	Bf	0.72	0.60	0.82	0.67
	Cf	0.57	0.65	0.79	0.73
	Df	0.77	0.47	0.79	0.66
Xuzhou-	Da	0.45	1.58	0.65	0.61

CUMT	Ca	0.59	0.96	0.71	0.82
	Ba	0.67	0.78	0.70	0.32
	Aa	0.73	0.78	0.82	0.49
	An	0.75	0.85	0.85	0.47
	Af	0.72	0.63	0.74	0.62
	Bf	0.62	0.65	0.75	0.53
	Cf	0.68	0.66	0.72	0.54
	Df	0.67	0.65	0.72	0.53

By comparing the validation results of MODIS AOD products with those of observation sites (Taihu: R=0.59, RMSE=0.19, $P<0.05$, RMB=0.52; Xuzhou-CUMT: R=0.71, RMSE=0.25, $P<0.05$, RMB=0.44) (Chen et al., 2021), we find that the improved MISR AOD has a higher correlation with MODIS AOD products in the Taihu and Xuzhou-CUMT sites. The smaller observation angle of the improved MISR AOD, the closer the error is to that of the MODIS AOD product. The observation angle of MISR An is the same as that of MODIS. Therefore, we selected An observation angle and MODIS AOD products at two pixel positions in Taihu and Xuzhou-CUMT for verification (Figure 9). The results show that the An AOD retrieval by the improved algorithm correlates well with the MODIS AOD product, and the position errors of the two image elements are close to each other. The RMSE of the Xuzhou-CUMT site is slightly higher than that of Taihu site, and the RMB of Taihu site is slightly higher than that of the Xuzhou-CUMT site.

5. Conclusion

This study first explored the problem of estimating the surface reflectance in our previous study. We obtained an error correction model for surface reflectance by using a linear fit of the MISR surface reflectance and a new estimate of the MISR surface reflectance. The improved MISR surface reflectance was obtained through the error correction model. We then retrieved a new AOD product using the improved surface reflectance and a lookup table constructed from the 6S model. Two AERONET ground observation sites with longer time series were used to validate the AOD obtained by satellites.

(1) Overall, the improved AOD and its spatial distribution trends are consistent with our previous results. The AOD estimated by our improved method exhibited higher accuracy and a high degree of agreement with the AERONET ground-based observational AOD.

(2) More importantly, compared to the MODIS AOD products, the retrieved AOD in this study has fewer missing AOD pixels and finer spatial resolution. The retrievals of An AOD by the improved algorithm are highly correlated with the MODIS AOD products, as shown through validation with the MODIS AOD product.

(3) In the future, more aerosol models that conform to the actual situation in the study area can be constructed using the AERONET ground observation data and introduced into the MISR AOD retrieval algorithm to further improve the accuracy of the AOD retrieval results. In this study, the AERONET AOD was used as the true value and as an input for the AOD parameter in the 6S model for atmospheric correction of MISR and MODIS images. We then obtained a surface reflectivity error correction model to retrieve the AOD for the entire region. It should be emphasized that the more AERONET sites used to train the corrected model, the more accurate the AOD results obtained by this method. However, the data from the AERONET ground observation sites were limited. In the future, the study area can be expanded on a large scale and for a longer time series.

Acknowledgement

This study was supported by the Key Program of the National Natural Science Foundation of

China (42130609), Jiangsu Funding Program for Excellent Postdoctoral Talent (2023ZB482), the Natural Science Foundation of Jiangsu Province of China (BK20220455), and the National Science Foundation of China (42201028).

Competing interests

The contact author has declared that none of the authors has any competing interests.

Reference

Berhane, S. A.; Bu, L. Aerosol-Cloud Interaction with Summer Precipitation over Major Cities in Eritrea[J]. Remote Sens-basel, 2021, 13(4):21.

Chen, L.; Wang, R.; Han J. Influence of observation angle change on satellite retrieval of aerosol optical depth[J]. Tellus B, 2021, 73.

Chen, L.; Fei, Y.; Wang, R. Retrieval of high temporal resolution aerosol optical depth using the GOCI remote sensing data[J]. Remote Sens-basel. 2021, 13:2376.

Chen, L.; Wang, R.; Wei, G. A surface reflectance correction model to improve the retrieval of MISR aerosol optical depth supported by MODIS data[J]. Adv Space Res, 2021, 67(2):858-867.

Dao, Y.; Gong, W. Observed holiday aerosol reduction and temperature cooling over East Asia[J]. J Geophys Res-atmos, 2014.

Daniel, R.; Steven, S.; Robert, W.; Leo, D. Climate Effects of Aerosol-Cloud Interactions[J]. Science, 2014, 343, 379-380.

Dehghani, M.; Saeedi, A. A.; Zamanian, Z. A study of the relationship between indoor and outdoor particle concentrations in Hafez hospital in Shiraz[J]. Phys.Rev.C, 2012.

Dong, W.; Tao, M.; Xu, X.; Wang, J.; Wang, Y.; Wang, L.; Song, Y.; Fan, M.; Chen, L. Satellite Aerosol Retrieval From Multiangle Polarimetric Measurements: Information Content and Uncertainty Analysis," IEEE Trans. Geosci. Remote Sens. 2023, 61, 1-13.

Dubovik, O.; Li.; Mishchenko M. I. Polarimetric remote sensing of atmospheric aerosols: Instruments, methodologies, results, and perspectives[J]. Pergamon, 2019, 474-511.

Deuzé, J. L.; Bréon, F. M.; Devaux, C.; Goloub, P.; Herman, M.; Lafrance, B.; Maignan, F.;

Marchand, A.; Nadal, F.; Perry, G.; Tanré, D. Remote sensing of aerosols over land surfaces from POLDER-ADEOS-1 polarized measurements. J Geophys Res-atmos, 2001, 106(D5): 4913-4926.

Flowerdew, R. J.; Haigh, J. D. Retrieval of aerosol optical thickness over land using the ATSR-2 Dual-look Satellite Radiometer. Geophys Res. Lett. 1996, 23 (4): 351-354.

Giles, D. M.; Sinyuk, A.; Sorokin, M. G. Advancements in the Aerosol Robotic Network (AERONET) Version 3 database-automated near-real-time quality control algorithm with improved cloud screening for Sun photometer aerosol optical depth (AOD) measurements[J]. Copernicus GmbH, 2019, 12(1), 169-209.

Gupta, P.; Levy, R. C.; Mattoo, S. A surface reflectance scheme for retrieving aerosol optical depth over urban surfaces in MODIS dark target retrieval algorithm[J]. Atmos Meas Tech, 2016, 9(7): 3293-3308.

Hatzianastassiou, N. The direct effect of aerosols on the radiation budget and climate of the Earth-atmosphere system: its variability in space and time. EGU General Assembly Conference Abstracts EGU General Assembly Conference Abstracts, 2009.

Holben, B. N.; Tanré, D.; Smirnov, A. An emerging ground-based aerosol climatology: Aerosol optical depth from AERONET[J]. J Geophys Res, 2001, 106, 12067-12097.

Huang X , Ding A .Aerosol as a critical factor causing forecast biases of air temperature in global numerical weather prediction models[J].Science Bulletin, 2021.DOI:10.1016/j.scib.2021.05.009.

Hsu, N. C.; Tsay, S. C.; King, M. D. Aerosol properties over bright-reflecting source regions[J]. IEEE Trans. Geosci. Remote Sens, 2004, 42(3):557- 569.

Kaufman, Yoram J. The MODIS 2.1-um channel--correlation with visible reflectance for use in remote sensing of aerosol.[J]. IEEE T Geosci Remote, 1997, 35, 1286-1298.

Kokhanovsky, A. A.; Curier, R. L.; Leeuw, G. D.; Grey, W. M. F. The intercomparison of AATSR dual-view aerosol optical thickness retrievals with results from various algorithms and instruments. Int. J. Remote Sens. 2009, 30 (17): 4525-4537.

Lee, S. S.; Donner L. J.; Penner J. E. Thunderstorm and stratocumulus: How does their contrasting morphology affect their interactions with aerosols?[J]. Atmos. Chem. Phys. 2010, 10(2), 6819-6837.

Li, E.; Zhang, Z.; Tan, Y. A Novel Cloud Detection Algorithm Based on Simplified Radiative Transfer Model for Aerosol Retrievals: Preliminary Result on Himawari-8 Over Eastern China[J]. IEEE T Geosci Remote, 2020, 59(3):1-12.

Li, Y.; Xue, Y.; Guang, J. Ground-Level PM2.5 Concentration Estimation from Satellite Data in the Beijing Area Using a Specific Particle Swarm Extinction Mass Conversion Algorithm[J]. Remote Sens-basel, 2018, 10(12), 1906.

Lu, S.; Xue, Y.; Yang, X.-H.; Leys, J.; Guang, J.; Che, Y.-H.; Fan, C.; Xie, Y.Q.; Li, Y. Joint Retrieval of Aerosol Optical Depth and Surface Reflflectance Over Land Using Geostationary Satellite Data. IEEE Trans. Geosci. Remote Sens. 2019, 57, 1489–1501.

Mironova, I. A. Aerosols over continental Portugal (1978-1993): their sources and an impact on the regional climate[J]. Atmos. Chem. Phys. 2015, 15(11):6407-6418.

Remer, L. A; Tanré, D.; Kaufman, Y. J. Algorithm for remote sensing of tropospheric aerosol from MODIS: Collection 005[J]. 2009.

Samset, B. H.; Sand, M.; Smith, C. J. Climate Impacts From a Removal of Anthropogenic Aerosol

Emissions[J]. Geophys Res Lett, 2018, 45(2).

Sun, E.; Fu, C.; Yu, W. Variation and Driving Factor of Aerosol Optical Depth over the South China Sea from 1980 to 2020[J]. Atmosphere, 2022, 13, 372.

Sundstrom, A. M.; Kolmonen, P.; Sogacheva, L.; Leeuw, G. D. Aerosol retrieval over China with the AATSR dual view algorithm. Remote Sens. Environ. 2012, 116 (1): 189-198.

Xie, Y.; Xue, Y.; Jie, G. Deriving a Global and Hourly Data Set of Aerosol Optical Depth Over Land Using Data From Four Geostationary Satellites: GOES-16, MSG-1, MSG-4, and Himawari-8[J].IEEE T Geosci Remote, 2019, 99:1-12.

Zhang, Y.; Li, Z.; Liu, Z. Retrieval of aerosol fine-mode fraction over China from satellite multiangle polarized observations: validation and comparison[J]. Atmos Meas Tech, 2021, 2, 1655-1672.